Superoxide Radical Anion Adduct of 5,5-Dimethyl-1-pyrroline *N*-Oxide (DMPO). 1. The Thermodynamics of Formation and Its Acidity

Frederick A. Villamena,*,† John K. Merle,‡ Christopher M. Hadad,*,‡ and Jay L. Zweier*,†

Center for Biomedical EPR Spectroscopy and Imaging, The Davis Heart and Lung Research Institute, and the Division of Cardiovascular Medicine, Department of Internal Medicine, College of Medicine, and Department of Chemistry, The Ohio State University, Columbus, Ohio 43210

Received: May 10, 2005

The nitrone 5,5-dimethyl-1-pyrroline *N*-oxide (DMPO) has been the most widely used spin trap for the detection of transient free radicals in chemical, biological, and biomedical research using electron paramagnetic resonance (EPR) spectroscopy. A density functional theory (DFT) approach was used to predict the thermodynamics of formation of the superoxide anion/hydroperoxyl radical ($O_2^{\bullet-}/{}^{\bullet}O_2H$) adduct of DMPO as well as its pK_a in aqueous systems. At the B3LYP/6-31+G(d,p)//B3LYP/6-31G(d) level, we predicted (in the gas phase and with a polarizable continuum model (PCM) for water) three conformational minima for both the DMPO−O_2^- and DMPO−O_2H adducts. Using DFT and the PCM solvation method, the pK_a of DMPO−O_2H was predicted to be 14.9 ± 0.5. On the basis of free energy considerations, the formation of DMPO−O_2H at neutral pH proceeds via initial addition of $O_2^{\bullet-}$ to DMPO to form the DMPO−O_2^- adduct and then subsequent protonation by water (or other acidic sources) to form DMPO−O_2H. Under acidic conditions, the addition of ${}^{\bullet}O_2H$ to DMPO is predicted to be more exoergic than the addition of $O_2^{\bullet-}$ and is consistent with available experimental kinetic data.

I. Introduction

The electron paramagnetic resonance (EPR) spin-trapping technique using nitrones as radical spin traps has been an indispensable tool in the detection of oxygen radical species (Scheme 1). The nitrone 5,5-dimethyl-1-pyrroline *N*-oxide (DMPO) was first synthesized in 1959 by Bonnett et al.[1] as a model compound toward the synthesis of corrins. Although Iwamura et al.[2] were the first to demonstrate the spin-trapping property of (*tert*-BuN(O)═CH)$_2$ with C-centered radicals, Janzen et al. reported in 1974 that DMPO can indeed be used to trap O-centered radicals.[3]

Prior to 1974,[4] the hydroperoxyl radical (${}^{\bullet}O_2H$) could only be detected directly by EPR at low temperature[5] or as a metal complex.[6,7] These approaches to radical detection limited the detection of superoxide ($O_2^{\bullet-}$) in biological systems, until DMPO was introduced for this purpose almost 3 decades ago by Harbor et al.[4] Subsequent detection of superoxide/hydroperoxyl ($O_2^{\bullet-}/{}^{\bullet}O_2H$) radicals in aqueous systems by EPR spin trapping using DMPO paved the way to exciting new findings in chemistry[8−12] and biology.[13−19]

Although DMPO is still widely employed as a spin trap, it has major drawbacks which limit the spectral interpretation of its adducts with $O_2^{\bullet-}/{}^{\bullet}O_2H$.[20−22] Several DMPO-type analogues have been developed over the years to overcome the limitation of DMPO. These DMPO-type spin traps include the alkoxyphosphorylated nitrones 5-diethoxyphosphoryl-5-methyl-1-pyrroline *N*-oxide (DEPMPO)[23−25] and 5-diisopropyloxyphosphoryl-5-methyl-1-pyrroline *N*-oxide (DIPPMPO)[26] and the alkoxycarbonyl-nitrones 5-ethoxycarbonyl-5-methyl-1-pyrroline *N*-oxide (EMPO)[27−30] and 5-butoxycarbonyl-5-methyl-1-pyrroline *N*-oxide (BocMPO).[30−33]

SCHEME 1: Spin Trapping by DMPO

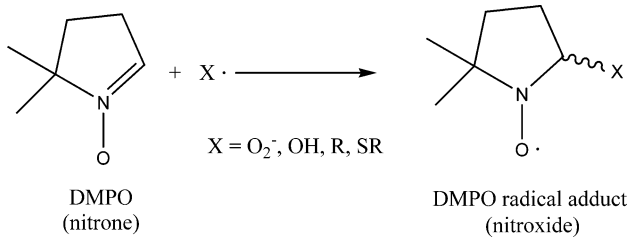

DMPO (nitrone) — DMPO radical adduct (nitroxide)

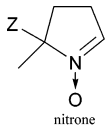

nitrone

nitrone	Z
DMPO	-Me
EMPO	-CO_2Et
BocMPO	-CO_2*t*-Bu
DEPMPO	-P(O)(OEt)$_2$
DIPPMPO	-P(O)(O*i*-Pr)$_2$

These substituted DMPO-type nitrones have demonstrated a relatively higher rate of superoxide ($O_2^{\bullet-}$) trapping as compared to that of DMPO.

The accurate interpretation of the nitrone−$O_2^{\bullet-}$/−O_2H adduct spectrum has confounded most spin-trapping researchers over the years because there has been no independently synthesized nitrone−O_2H (or nitrone−O_2^-) to date, and it is virtually impossible to deduce its actual form and property in solution due to its low concentration after spin trapping. In this paper, DMPO will be used as a simple model to understand the

* To whom correspondence should be addressed. E-mail: villamena-1@medctr.osu-edu (F.A.V.); hadad.1@osu.edu (C.M.H.); zweier-1@medctr.osu.edu (J.L.Z.). Fax: (614)-292-8454 (F.A.V.); (614)-292-1685 (C.M.H.); (614)-247-7799 (J.L.Z.).

† The Davis Heart and Lung Research Institute and College of Medicine.

‡ Department of Chemistry.

10.1021/jp052431f CCC: $30.25
Published on Web 06/17/2005

TABLE 1: Comparison of Selected X-ray Crystallographic and Calculated Bond Lengths from Various Levels of Theory[a]

bonds	calculated bond distance range (Å)	experimental bond distances (Å)
nitronyl C=N	1.31	1.291(2);[53] 1.307(2)[54]
nitronyl N−O	1.26	1.2987(16);[53] 1.294(1)[54]
nitroxyl C−N	1.45−1.50	1.50[55]
nitroxyl N−O	1.27−1.29	1.27[55]
	O_2 Adduct	
C_{ring}−O_2	1.36−1.39	1.441(2)[56]
O−O	1.45−1.49	1.4599(17)[56]
	O_2H Adduct	
C_{ring}−O_2H	1.41−1.46	1.441(2)[56]
O−O	1.44−1.46	1.4599(17)[56]
O−H	0.96−0.98	1.02(3)[56]

[a] The B3LYP/6-31G(d), B3LYP/6-311+G(d), B3LYP/6-311+G(d,p), and B3LYP/aug-cc-pVDZ levels of theory.

chemistry underlying the spin-trapping process, that is, the most plausible mechanism of $O_2^{\bullet-}$ trapping by DMPO. Theoretical evidence will be presented as to whether the DMPO−O_2^- adduct can exist as the anionic or neutral form in aqueous solution, and if the DMPO−O_2^- adduct does exist as DMPO−O_2H, then what is the latter's approximate pK_a? We now present the thermodynamics of formation and acidity of the superoxide radical adduct of DMPO. A companion paper[34] will present proposed pathways for the decay of these adducts.

II. General Computational Methods

Density functional theory (DFT)[35,36] was applied in this study to determine the optimized geometry, vibrational frequencies, and single-point energy of all stationary points.[37−40] The effect of solvation on the gas-phase calculations was also investigated using the polarizable continuum model (PCM).[41−45] All calculations were performed using Gaussian 98[46] or Gaussian 03[47] at the Ohio Supercomputer Center. Single-point energies were obtained at the B3LYP/6-31+G(d,p) level based on the optimized B3LYP/6-31G(d) geometries, unless otherwise indicated. The minima for both the nitrone spin traps and $O_2^{\bullet-}$/$^{\bullet}O_2H$ adducts have zero imaginary vibrational frequencies as derived from a vibrational frequency analysis (B3LYP/6-31G(d)). A scaling factor of 0.9806 was used[48] for the zero-point vibrational energy (ZPE) corrections. Spin contamination for all stationary points of the $O_2^{\bullet-}$/$^{\bullet}O_2H$ adduct structures was negligible, that is, $0.75 < \langle S^2 \rangle < 0.76$. In some cases, the CBS-Q[49] and CBS-QB3[50,51] methods were used for comparison of the B3LYP calculations to energies at the infinite basis set and electron correlation limit.

III. Optimal Geometry Search

To understand the structures of the adducts between $O_2^{\bullet-}$/$^{\bullet}O_2H$ with DMPO, we utilized computational methods to probe the geometric preferences. All bond lengths and angles for DMPO, DMPO−O_2^-, and DMPO−O_2H at their optimized geometries using the B3LYP/6-31G(d), B3LYP/6-311+G(d), B3LYP/6-311+G(d,p), and B3LYP/aug-cc-pVDZ[52] levels of theory have been extensively examined, and in general, these results showed no significant deviation from those reported experimentally using X-ray crystallography, as shown in Table 1. The calculated O−O distances for $O_2^{\bullet-}$ and $^{\bullet}O_2H$ are 1.35 and 1.33 Å, respectively, while the O−H distance in $^{\bullet}O_2H$ is 0.98 Å at the B3LYP/6-31G(d) level of theory.

Model geometries for the DMPO−O_2^- and DMPO−O_2H adducts were explored. Figure 1 shows the energy profile of

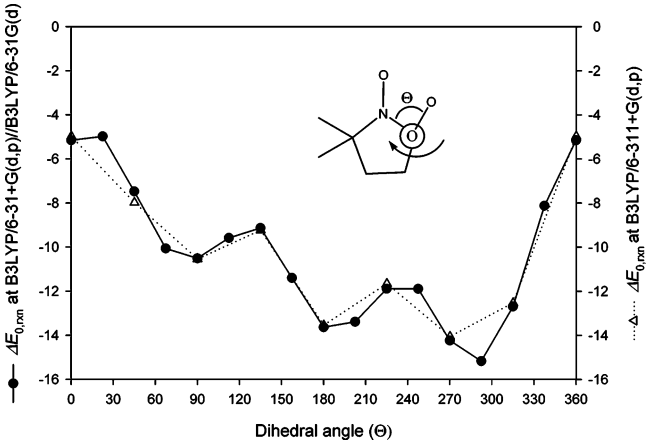

Figure 1. Rotational barriers in the DMPO−O_2^-adduct. The dihedral angles are at 22.5° increments along the N−C−O−O angle as a function of the bottom-of-the-well energies ($\Delta E_{0,rxn}$) in kilocalories per mole at the B3LYP/6-31+G(d,p)//B3LYP/6-31G(d) (●) and B3LYP/6-311+G(d,p) (△) levels of theories.

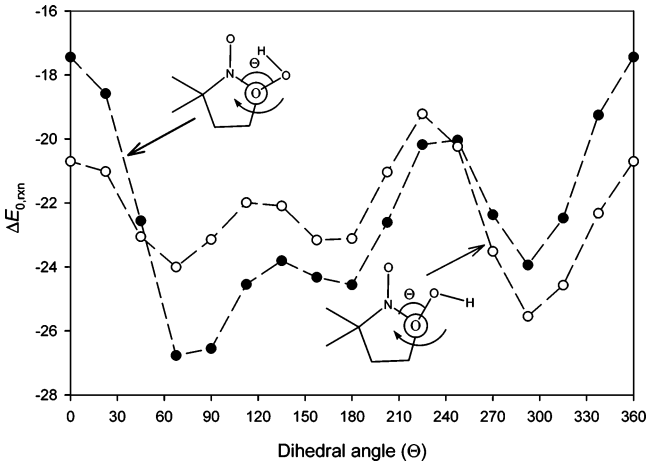

Figure 2. Rotational barriers in the DMPO−O_2H adduct. The dihedral angles are at 22.5° increments along the N−C−O−O angle as a function of the bottom-of-the-well reaction energies at the B3LYP/6-31+G(d,p)//B3LYP/6-31G(d) level of theory: conformation A (●); conformation B (○) (see text for diagram).

the bottom-of-the-well reaction energies ($\Delta E_{0,rxn}$) for the formation of DMPO−O_2^- as a function of the N−C−O−O dihedral angles at the B3LYP/6-31+G(d,p)//B3LYP/6-31G(d) and (fully optimized) B3LYP/6-311+G(d,p) levels of theory. Geometry optimizations with diffuse functions using the B3LYP/6-311+G(d,p) level of theory were performed to account for the negative charge character of the DMPO−O_2^- adduct. The optimized DMPO−O_2^- geometries in the absence and presence of the diffuse function show very similar trends in the final energetics with various D(N−C−O−O) dihedral angles. Three local minima were located corresponding to fixed D(N−C−O−O) angles of 90, 180, and 292.5° at the B3LYP/6-31G(d) level, while optimization of these starting geometries at the B3LYP/6-311+G(d,p) level without constraints gave final D(N−C−O−O) angles of 81.9, 186.9, and 292.5°, respectively. The most thermodynamically favored conformation for DMPO−O_2^- was found to have a D(N−C−O−O) angle of ∼292°.

Geometry searches for the DMPO−O_2H adduct at the B3LYP/6-31+G(d,p)//B3LYP/6-31G(d) level were performed, and they yielded two major conformations (denoted as A and B) which are dominated by the orientation of the hydroperoxyl H relative to the N−O moiety, as shown in Figure 2. The dihedral angle (Θ) on the N−C−O−O bond was once again

varied at 22.5° increments for each of the main conformations, and then, full geometry optimization was performed for the local minima. Conformation A gave three relaxed geometries with $\Theta = 75.9$ (with a N−O• • •H−OO intramolecular H-bonding distance of 2.00 Å), 174.3, and 294.6°. Optimization of structures with conformation B also gave three relaxed geometries at $\Theta = 299.7$ (with N−O• • •H−OO of 3.09 Å), 172.3, and 65.4°. The formation of the most favored structure for conformation B ($\Theta = 299.7°$) is less exothermic than that of the most favored structure with conformation A ($\Theta = 75.9°$). Interestingly, single-point energy analysis in the aqueous phase at the PCM B3LYP/6-31+G(d,p) level using the B3LYP/6-31G(d) optimized geometries for both DMPO−O_2^- and DMPO−O_2H (both conformations A and B) did not follow the same energy profile as in the gas-phase energies at the B3LYP/6-31+G(d,p)//B3LYP/6-31G(d) level (see Supporting Information Figure S1). Optimization using B3LYP/6-311+G(d,p) of the A and B conformations at $\Theta = 67.5$, 180, and 292.5° initial geometries only provided final structures of the A conformation with $\Theta = 78.0$ and 173.0° and of the B conformation with $\Theta = 66.2$ and 296.3°. The $\Delta G_{solv,298K}$ values for DMPO−O_2H are the following: −10.3 ($\Theta = 78.0°$) and −12.5 ($\Theta = 173.0°$) kcal/mol for the A conformation and −15.0 ($\Theta = 66.2°$) and −14.1 ($\Theta = 296.3°$) kcal/mol for the B conformation at the PCM/B3LYP/6-311+G(d) level. The calculated free energies of solvation ($\Delta G_{solv,298K}$) at the PCM/B3LYP/6-311+G(d) level for DMPO−O_2^- at $\Theta = 81.9$, 186.9, and 292.5° are −65.2, −64.6, and −60.0 kcal/mol, respectively. The large free energy of solvation is reasonable for the anionic species.

To test the accuracy of the level of theory employed in our study, we compared the experimental O−H bond dissociation energy of 2,2,6,6-tetramethylpiperdine *N*-hydroxyl (TEMPO−H) with the theoretically predicted enthalpy values at the B3LYP/6-31+G(d,p)//B3LYP/6-31G(d), CBS-Q, and CBS-QB3 levels of theory.

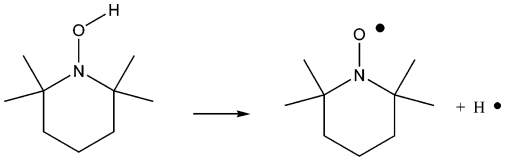

The results show that the calculated ΔH(298 K) values at the B3LYP/6-31+G(d,p)//B3LYP/6-31G(d), CBS-Q, and CBS-QB3 levels of theory are 64.7, 69.1, and 70.1 kcal/mol, respectively. The two CBS values are in very good agreement with the experimental value of 69.6 kcal/mol as reported by Mahoney et al.[57] The B3LYP value is about 4 kcal/mol lower than the experimental value, and this apparent discrepancy may be due to an underestimation of the *N*-oxyl energy at the B3LYP/6-31+G(d,p)//B3LYP/6-31G(d) level. (A further comparison of these theoretical methods for computing an accurate Boltzmann distribution will be presented in our companion paper.[34])

IV. Approximation of the pK_a of the O_2•−/•O_2H Adduct

The theoretical elucidation of the preferred structure of DMPO $O_2^{\bullet-}$/•O_2H in water is important not only for an understanding of the mechanistic aspects of $O_2^{\bullet-}$ trapping by DMPO but also to serve as models for calculation of the EPR hyperfine coupling constants (hfcc's) to compare directly with experiment. We addressed a few specific questions.

First, is the superoxide adduct protonated at neutral pH? To provide an estimate of the relevant pK_a, optimized geometries were obtained, and harmonic vibrational frequency analyses were performed on various acids and their conjugate bases at the B3LYP/6-311+G(d) level. Approximation of the pK_a of HNO,[58] amides,[59] aliphatic alcohols, and carboxylic acids[60,61] has been performed using the free energy (in aqueous solution), as obtained with the polarizable continuum model (PCM).[62] All preferred conformations of the carboxylic acid groups are in the *Z* form, as is well-known experimentally.[63,64] Estimation of the pK_a values was also extended to the paramagnetic molecule, 3-carboxy-PROXYL (CP) using the PCM method.[65]

TABLE 2: Calculated and Experimental pK_a Values and Their Respective Deprotonation Energies and Solvation Energies

acid	$\Delta G_{(gas)}$[a] (kcal/mol)	$\Delta G_{(solv)}$[b] (kcal/mol)	reported pK_a[c]	calculated pK_a[d]
trifluoroacetic acid	314.6	−59.9	0.2	0.2
trichloroacetic acid	312.7	−60.9	0.7	−1.5
dinitromethane	314.9	−53.8	3.6	3.6
formic acid	335.6	−74.8	3.8	3.4
acrylic acid	337.0	−71.5	4.3	5.9
acetic acid	340.6	−73.4	4.8	6.9
hydrogen cyanide	346.4	−79.6	9.2	6.6
phenol	341.5	−70.4	10	8.9
methylthiol	352.0	−74.9	10.3	12.2
allyl alcohol	366.3	−86.0	15.5	13.9
methanol	373.9	−92.2	15.5	14.7
water	384.7	−103.3	15.7	14.4
acetone	366.8	−73.1	19.3	21.1
acetonitrile	370.2	−70.1	25	24.6
H_3CO_2H	365.3	−87.4	11.5[66]	12.6
hydroperoxyl radical	344.5	−85.6	4.8[67]	2.4
Cl_3CCO_2H	330.6	−67.5	8.7[68]	4.7
PhO_2H	346.2	−74.7	8.9[68]	9.2
$HOCH_2O_2H$	356.8	−76.4	10.7[68]	14.0
tert-BuO_2H	363.7	−83.4	12.8[66]	13.9
hydrogen peroxide	368.8	−90.3	11.65[66]	12.9
CP	329.2	−59.3	4.0[65]	8.3
DMPO−O_2H[e]				
78° → 81.9°	357.6	−74.9		15.2
78° → 186.9°	354.7	−73.6		14.3
78° → 292.5°	353.7	−70.7		15.3

[a] Bottom-of-the-well energy plus scaled ZPE at the B3LYP/6-311+G(d) level. [b] Bottom-of-the-well energy using the B3LYP/6-311+G(d) and PCM/B3LYP/6-311+G(d) levels. [c] Taken from ref 58, unless otherwise indicated. [d] From the linear regression pK_a = $0.538(\Delta G_{aq,AH}) - 136.9$ including hydroperoxides and nitroxides ($r^2 = 0.95$ and $\sigma = 0.8$ pK_a units). [e] These values are N−C−O−O dihedral angles in which 78° corresponds to DMPO−O_2H and 81.9, 186.9, and 292.5° are for DMPO−O_2^-.

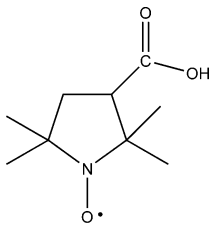

CP

Table 2 shows the calculated pK_a values which are based on the following relationship:

$$pK_a = 0.538(\Delta G_{aq,AH}) - 136.9$$

derived from all compounds listed in the table including compounds with peroxyl and nitroxyl moieties. The calculated $\Delta G_{(gas)}$ values for some of the compounds reported by Bartberger et al.[58] are reproducible up to 0.1 kcal/mol except for

TABLE 3: Calculated Thermodynamic Parameters[a] for the Formation of the Hydroperoxyl−DMPO Adduct in the Gas and Aqueous Phases

Mechanism A

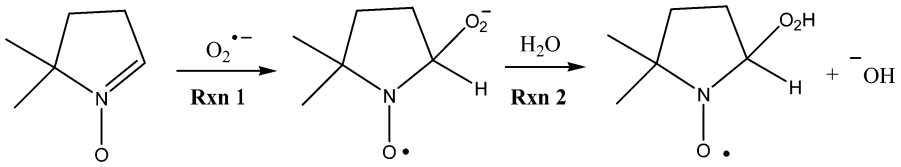

	$\Delta E_{0,rxn}$[b]	$\Delta H_{298,rxn}$	$\Delta G_{298,rxn}$
Gas Phase			
Rxn 1	-15.4	-14.6	-4.0
Rxn 2	29.8	30.3	31.3
Aqueous Phase			
Rxn 1	6.1	6.7	16.8
Rxn 2	3.3	3.9	5.0

Mechanism B

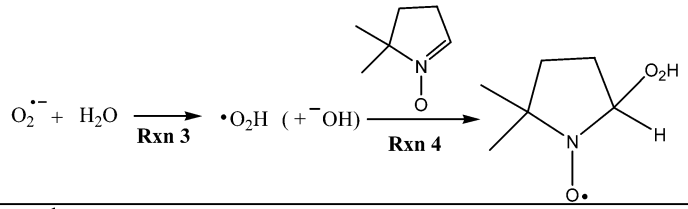

	$\Delta E_{0,rxn}$[b]	$\Delta H_{298,rxn}$	$\Delta G_{298,rxn}$
Gas Phase			
Rxn 3	41.1	40.2	39.9
Rxn 4	-26.7	-24.4	-12.6
Aqueous Phase			
Rxn 3	33.0	32.1	31.9
Rxn 4	-23.6	-21.5	-10.1

[a] All energies are in kilocalories per mole at the B3LYP/6-311+G(d) (gas) and PCM/B3LYP/6-311+G(d)//B3LYP/6-311+G(d) levels of theory. Values are based on the most stable conformations of the DMPO−O_2^- and DMPO−O_2H adducts in each phase. [b] Bottom-of-the-well energy.

the allyl alcohol (366.3 kcal/mol) with a 0.5 kcal/mol difference as compared to the previously calculated value 365.8 kcal/mol. The pK_a values of hydroperoxyl compounds were estimated, and these gave values that correlate well with the corresponding experimental pK_a data (Supporting Information Figure S2). The standard deviation for the pK_a of the peroxyl compounds is 1.0 pK_a units, while that of the nitroxide CP gave a standard deviation of about 3.1 pK_a units compared to the overall standard deviation of 0.8 pK_a units.

The pK_a value of DMPO−O_2H was approximated from the preferred conformation of DMPO−O_2H ($\Theta = 78°$) and from the three conformations of DMPO−O_2^- ($\Theta = 81.9$, 186.9, and 292.5°). Values of pK_a = 15.2, 14.3, and 15.3 corresponding to Θ (DMPO−O_2^-) = 81.9, 186.9, and 292.5°, respectively, were obtained with an average value of 14.9 ± 0.5. This pK_a value of 14.9 is close to that observed experimentally from alcohols with pK_a values ranging from 15.5 to 17.1 and water of 15.7.[58,69]

V. Thermodynamics of Superoxide Radical Trapping

On the basis of the derived pK_a for DMPO−O_2H of 14.9 ± 0.5, the hydroperoxyl form of the adduct should be the observed form in the aqueous phase at neutral pH. Also, it is clear that, at neutral pH, the major form of the superoxide reactant is the anionic form, since the experimental pK_a for $^\bullet O_2$H is 4.8[67] (or 4.4[70]). Moreover, the rate constant for the dissociation of $^\bullet O_2$H is approximately 10^6 s^{-1}, as reported by Bielski and Czapski;[70] hence, the rate constant for the association of H^+ and $O_2^{\bullet-}$ has to be on the order of 10^{10} M^{-1} s^{-1}. The higher equilibrium concentration of $O_2^{\bullet-}$ compared to $^\bullet O_2$H at neutral pH is consistent with the experimental reduction potentials of $E° = 1.06$ and 0.94 V for $^\bullet O_2$H and $O_2^{\bullet-}$, respectively.[71] However, a question still remains as to whether $O_2^{\bullet-}$ or $^\bullet O_2$H is initially trapped by DMPO in aqueous solution.

An important reason for considering $^\bullet O_2$H as the species being trapped is that $^\bullet O_2$H appears to be more reactive than $O_2^{\bullet-}$ on the basis of the trapping rates at different pHs. The rate constants for $O_2^{\bullet-}$ addition to DMPO were reported to be 10 M^{-1} s^{-1} at

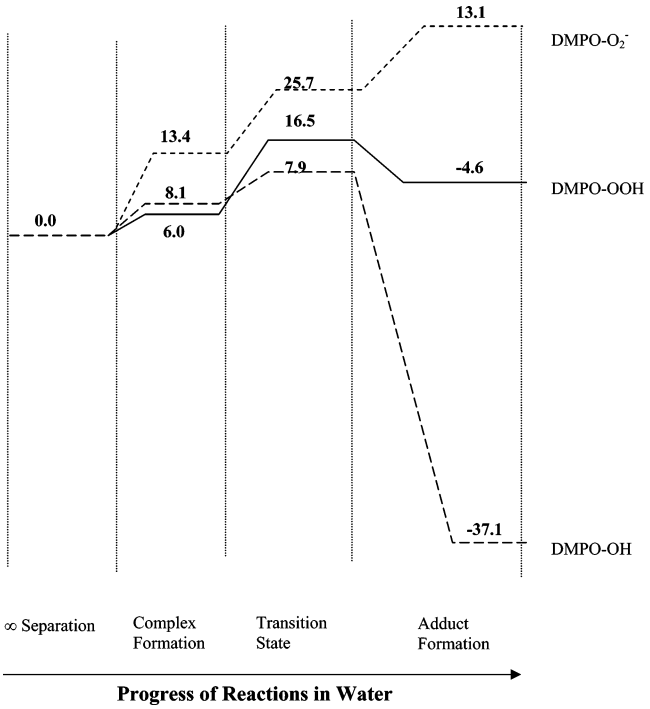

Figure 3. Schematic diagram of the DMPO reaction with $O_2^{\bullet-}$, $^{\bullet}O_2H$, and •OH in the aqueous phase including the transition state [DMPO-radical]‡ for the radical adduct formation. The values are free energies (ΔG_{298}) in kilocalories per mole obtained at the B3LYP/6-31+G(d,p)//B3LYP/6-31G(d) level (see Table 4 for a complete list of energies).

TABLE 4: Calculated Relative Enthalpies (ΔH^{298K}) and Free Energies (ΔG^{298K}) (kcal/mol) in the Gas and Aqueous Phases (in Parentheses) and Other Theoretical Parameters for the Transition-State Structures of the $^{\bullet}O_2H$, $O_2^{\bullet-}$, and $^{\bullet}OH$ Adducts at the B3LYP/6-31+G(d,p)//B3LYP/6-31G(d) Level

structure	ΔH^{298K} [a]	ΔG^{298K} [a]	C···O−X (Å)	$\langle S^2\rangle$ [b]	N_{imag} [c]
		•OH			
DMPO + •OH[d]	0.0 (0.0)	0.0 (0.0)	∞	0.00	0
DMPO−OH[e]	−9.8 (−1.8)	0.2 (8.1)	3.20	0.75	0
DMPO−OH TS[f]	−8.3 (−2.4)	2.1 (7.9)	2.78	0.75	1
DMPO−OH	−55.0 (−50.2)	−41.9 (−37.1)	1.40	0.75	0
		$O_2^{\bullet-}$			
DMPO + $O_2^{\bullet-}$	0.0 (0.0)	0.0 (0.0)	∞	0.00	0
DMPO−O_2^-	−15.9 (4.3)	−6.8 (13.4)	2.79	0.76	0
DMPO−O_2^- TS[g]	−3.3 (15.6)	6.8 (25.7)	1.81	0.78	1
DMPO−O_2^-	−13.9 (1.8)	−2.6 (13.1)	1.42	0.75	0
		$^{\bullet}O_2H$			
DMPO + $^{\bullet}O_2H$	0.0 (0.0)	0.0 (0.0)	∞	0.00	0
DMPO−O_2H	−13.8 (−5.1)	−2.7 (6.0)	3.55	0.75	0
DMPO−O_2H TS[g]	−3.0 (3.9)	9.7 (16.5)	2.10	0.79	1
DMPO−O_2H	−27.3 (−19.1)	−12.8 (−4.6)	1.38	0.75	0

[a] The values in parentheses are relative energies based on single-point energy calculations with the polarizable continuum model (PCM) at the B3LYP/6-31+G(d,p) level using water as a solvent. [b] The $\langle S^2\rangle$ value for all of the nitrones is 0.00, while that of the radicals is 0.75. [c] The point group for all structures is C_1, and N_{imag} refers to the number of imaginary vibrational frequencies (1 = TS). [d] At infinite separation. [e] Nitrone−R complex (R = OH, O_2H, or O_2). [f] TS stands for transition state. [g] On the basis of the DMPO−O_2^- and DMPO−O_2H structures with D(N−C−O−O) angles of ∼290 and ∼76°, respectively.

pH 7 and 6600 M^{-1} s^{-1} at pH 5.[72] Similarly, $O_2^{\bullet-}$ addition to 5-*tert*-butoxycarbonyl-5-methyl-1-pyrroline *N*-oxide (BMPO or BocMPO) has been reported to occur with a k_{app} value of 75.0 M^{-1} s^{-1} at pH values above 7.0 and 239 M^{-1} s^{-1} at pH 5.0.[31] A likely explanation for these faster rates in more acidic media is that a higher proportion of the more reactive $^{\bullet}O_2H$ is present.

To give further insight into which form of the radical is trapped, the thermodynamics in the aqueous and gaseous phases were considered. The results of those calculations (at the B3LYP/6-31+G(d,p)//B3LYP/6-31G(d) level) are shown in Table 3 for the direct trapping of $O_2^{\bullet-}$ (mechanism A) and for the trapping of $^{\bullet}O_2H$ formed after protonation of $O_2^{\bullet-}$ by water (mechanism B). Of course, since these mechanisms differ only by the sequences of steps, the overall ΔG must be the same and provides values of 27.3 kcal/mol for the gas phase and 21.8 kcal/mol for the aqueous phase (PCM). However, inspection of the separate steps shows clearly that mechanism A is preferred. The overall ΔG value 21.8 kcal/mol in the aqueous phase results from two endoergic steps: 16.8 kcal/mol for direct trapping of $O_2^{\bullet-}$ and 5.0 kcal/mol for the subsequent protonation of the anionic adduct. In mechanism B, the value 21.8 kcal/mol derives from a large endoergic step of 31.9 kcal/mol for the formation of $^{\bullet}O_2H$ combined with a subsequent exoergic (−10.1 kcal/mol) trapping step to form the final adduct. A similar set of results was obtained for the gas-phase calculations.

In addition to showing that trapping of $O_2^{\bullet-}$ is the most likely mechanism, the data of Table 3 are important in understanding why $^{\bullet}O_2H$ is more reactive than $O_2^{\bullet-}$. The aqueous ΔG values for the trapping event that occurs in mechanism A, step 1 (16.8 kcal/mol), versus mechanism B, step 4 (−10.1 kcal/mol), reveal that adduct formation with $^{\bullet}O_2H$ is more thermodynamically favored by 20 kcal/mol than adduct formation with $O_2^{\bullet-}$. Of course, these calculations relate to water at neutral pH, and as the pH decreases or with more potent acid sources (e.g., thiols, ammonium ions, or ascorbic acid), mechanism B may be facilitated in biological systems.

Figure 3 and Table 4 show the free energies and enthalpies of the transition-state structures as well as the products for the formation of the $^{\bullet}OH$, $O_2^{\bullet-}$, and $^{\bullet}O_2H$ adducts of DMPO. The calculated gas-phase free energy of activation barriers are 2.3, 0.0, and 7.0 kcal/mol for the addition of $^{\bullet}OH$, $O_2^{\bullet-}$, and $^{\bullet}O_2H$ to DMPO, respectively. In the gas phase, the order of decreasing exoergicity (kilocalories per mole) for the overall addition reaction of various radicals to DMPO is the following: $^{\bullet}OH$ (−41.9) < $^{\bullet}O_2H$ (−12.8) < $O_2^{\bullet-}$ (−2.6). However, it is to be expected that solvation will play a significant role in this addition process, especially considering the anionic character of the superoxide potential energy surface. Therefore, we employed single-point energy calculations with the PCM method at the B3LYP/6-31+G(d,p) level using water as a solvent (see Table 4) for the addition processes of $^{\bullet}OH$, $^{\bullet}O_2H$, and $O_2^{\bullet-}$. Worth noting is that the aqueous-phase addition of $O_2^{\bullet-}$ to DMPO is endoergic by 13.1 kcal/mol and occurs with a high free energy of activation barrier (ΔG(289K,aq)) of 25.7 kcal/mol as compared to the $\Delta G^{\ddagger}$(289K,aq) activation barriers for the addition of $^{\bullet}OH$ (7.9 kcal/mol) and $^{\bullet}O_2H$ (16.5 kcal/mol). These calculated activation energies are very consistent with the experimentally observed kinetic data[31,33,72,73] which confirm the slow trapping of $O_2^{\bullet-}$ by nitrones.

VI. Conclusions

A conformational search of DMPO−O_2H and DMPO−O_2^- adducts in the gas and aqueous phases gave three local minima for each adduct. These energy minima, together with optimized structures of various acids and hydroperoxyl compounds, were used to calculate the pK_a of DMPO−O_2H. The predicted pK_a for DMPO−O_2H was estimated to be 14.9 ± 0.5, and DMPO−O_2H should exist in its neutral form in aqueous solution at pH 7.

Thermodynamically, the preferred mechanism for the formation of DMPO−O_2H in gas and in water involves the initial

addition of $O_2^{\bullet-}$ to DMPO and subsequent protonation of the DMPO−O_2^- adduct. The addition of $^{\bullet}O_2H$ to DMPO is predicted to be more exoergic than the addition of $O_2^{\bullet-}$, which accounts for the higher rate constant of superoxide adduct formation in acidic pH.

Acknowledgment. The authors wish to thank The Ohio Supercomputer Center (OSC) for support of this research and Prof. DeLanson R. Crist (Georgetown) and Dr. Micheal Bartberger (Amgen) for valuable suggestions. This work was supported by NIH grants HL38324, HL63744, and HL65608. C.M.H. acknowledges support from the NSF-funded Environmental Molecular Science Institute (CHE-0089147). J.K.M. acknowledges support from an Amoco fellowship.

Supporting Information Available: Energies, enthalpies, and free energies for all spin traps and their corresponding spin adducts and complete refs 46 and 47. This material is available free of charge via the Internet at http://pubs.acs.org.

References and Notes

(1) Bonnett, R.; Brown, R. F. C.; Clark, V. M.; Sutherland, I. O.; Todd, A. *J. Chem. Soc., Abstr.* **1959**, 2094−2102.
(2) Iwamura, M.; Inamoto, N. *Bull. Chem. Soc. Jpn.* **1967**, *40*, 703.
(3) Janzen, E. G.; Evans, C. A. *J. Am. Chem. Soc.* **1973**, *95*, 8205.
(4) Harbour, J. R.; Chow, V.; Bolton, J. R. *Can. J. Chem.* **1974**, *52*, 3549−3553.
(5) Adrian, F. J.; Cochran, E. L.; Bowers, V. A. *J. Chem. Phys.* **1967**, *47*, 5441−5442.
(6) Meisel, D.; Levanon, H.; Czapski, G. *J. Phys. Chem.* **1974**, *78*, 779−782.
(7) Saito, E.; Bielski, B. H. J. *J. Am. Chem. Soc.* **1961**, *83*, 4467−4468.
(8) Yamakoshi, Y.; Sueyoshi, S.; Fukuhara, K.; Miyata, N.; Masumizu, T.; Kohno, M. *J. Am. Chem. Soc.* **1998**, *120*, 12363−12364.
(9) Makino, K.; Mossoba, M. M.; Riesz, P. *J. Am. Chem. Soc.* **1982**, *104*, 3537−3539.
(10) Stoyanovsky, D. A.; Clancy, R.; Cederbaum, A. I. *J. Am. Chem. Soc.* **1999**, *121*, 5093−5094.
(11) Jones, C. M.; Burkitt, M. J. *J. Am. Chem. Soc.* **2003**, *125*, 6946−6954.
(12) Pryor, W. A.; Terauchi, K.; Davis, W. H. J. *Environ. Health Perspect.* **1976**, *16*, 161−176.
(13) Pou, S.; Pou, W. S.; Bredt, D. S.; Snyder, S. H.; Rosen, G. M. *J. Biol. Chem.* **1992**, *267*, 24173−24176.
(14) Harbour, J. R.; Bolton, J. R. *Biochem. Biophys. Res. Commun.* **1975**, *64*, 803−807.
(15) Xia, Y.; Zweier, J. L. *Proc. Natl. Acad. Sci. U.S.A.* **1997**, *94*, 6954−6958.
(16) Rosen, G. M.; Britigan, B. E.; Cohen, M. S.; Ellington, S. P.; Barber, M. J. *Biochim. Biophys. Acta* **1988**, *969*, 236−241.
(17) Chamulitrat, W.; Hughes, M. F.; Eling, T. E.; Mason, R. P. *Arch. Biochem. Biophys.* **1991**, *290*, 153−159.
(18) Zweier, J. L. *J. Biol. Chem.* **1988**, *263*, 1353−1357.
(19) Zweier, J. L.; Kuppusamy, P.; Lutty, G. A. *Proc. Natl. Acad. Sci.* **1988**, *85*, 4046−4050.
(20) Buettner, G. R.; Oberley, L. W. *Biochem. Biophys. Res. Commun.* **1978**, *83*, 69−74.
(21) Finkelstein, E.; Rosen, G. M.; Rauckman, E. J. *Mol. Pharm.* **1982**, *21*, 262−265.
(22) Pou, S.; Hassett, D. J.; Britigan, B. E.; Cohen, M. S.; Rosen, G. M. *Anal. Biochem.* **1989**, *177*, 1−6.
(23) Frejaville, C.; Karoui, H.; Tuccio, B.; Le Moigne, F.; Culcasi, M.; Pietri, S.; Lauricella, R.; Tordo, P. *J. Med. Chem.* **1995**, *38*, 258−265.
(24) Liu, K. J.; Miyake, M.; Panz, T.; Swartz, H. *Free Radical Biol. Med.* **1999**, *26*, 714−721.
(25) Stolze, K.; Udilova, N.; Nohl, H. *Free Radical Biol. Med.* **2000**, *29*, 1005−1014.
(26) Chalier, F.; Tordo, P. *J. Chem. Soc., Perkin Trans. 2* **2002**, 2110−2117.
(27) Olive, G.; Mercier, A.; Le Moigne, F.; Rockenbauer, A.; Tordo, P. *Free Radical Biol. Med.* **2000**, *28*, 403−408.
(28) Zhang, H.; Joseph, J.; Vasquez-Vivar, J.; Karoui, H.; Nsanzumuhire, C.; Martasek, P.; Tordo, P.; Kalyanaraman, B. *FEBS Lett* **2000**, *473*, 58−62.
(29) Stolze, K.; Udilova, N.; Nohl, H. *Biol. Chem.* **2002**, *383*, 813−820.
(30) Stolze, K.; Udilova, N.; Rosenau, T.; Hofinger, A.; Nohl, H. *Biol. Chem.* **2003**, *384*, 493−500.
(31) Tsai, P.; Ichikawa, K.; Mailer, C.; Pou, S.; Halpern, H. J.; Robinson, B. H.; Nielsen, R.; Rosen, G. M. *J. Org. Chem.* **2003**, *68*, 7811−7817.
(32) Zhao, H.; Joseph, J.; Zhang, H.; Karoui, H.; Kalyanaraman, B. *Free Radical Biol. Med.* **2001**, *31*, 599−606.
(33) Villamena, F.; Zweier, J. *J. Chem. Soc., Perkin Trans. 2* **2002**, 1340−1344.
(34) Villamena, F. A.; Merle, J. K.; Hadad, C. M.; Zweier, J. L. *J. Phys. Chem. A* **2005**, *109*, 6089−6098.
(35) Labanowski, J. W.; Andzelm, J. *Density Functional Methods in Chemistry*; Springer: New York, 1991.
(36) Parr, R. G.; Yang, W. *Density Functional Theory in Atoms and Molecules*; Oxford University Press: New York, 1989.
(37) Hehre, W. J.; Radom, L.; Schleyer, P. V.; Pople, J. A. *Ab Initio Molecular orbital Theory*; John Wiley & Sons: New York, 1986.
(38) Becke, A. D. *Phys. Rev. A* **1988**, *38*, 3098.
(39) Becke, A. D. *J. Chem. Phys.* **1993**, *98*, 5648.
(40) Lee, C.; Yang, W.; Parr, R. G. *Phys. Rev. B* **1988**, *37*, 785.
(41) Tomasi, J.; Persico, M. *Chem. Rev.* **1994**, *94*, 2027.
(42) Cossi, M.; Barone, V.; Cammi, R.; Tomasi, J. *Chem. Phys. Lett.* **1996**, *255*, 327.
(43) Barone, V.; Cossi, M.; Tomasi, J. *J. Chem. Phys.* **1997**, *107*, 3210.
(44) Barone, V.; Cossi, M.; Tomasi, J. *J. Comput. Chem.* **1998**, *19*, 404.
(45) Cossi, M.; Barone, V. *J. Chem. Phys.* **1998**, *109*, 6246.
(46) Frisch, M. J.; et al. *Gaussian 98*, revision A.11.3; Gaussian, Inc.: Pittsburgh, PA, 2002.
(47) Frisch, M. J.; et al. *Gaussian 03*, revision B.04; Gaussian, Inc.: Pittsburgh, PA, 2003.
(48) Scott, A. P.; Radom, L. *J. Phys. Chem.* **1996**, *100*, 16502−16513.
(49) Ochterski, J. W.; Petersson, G. A.; Montgomery, J. A., Jr. *J. Chem. Phys.* **1996**, *104*, 2598.
(50) Montgomery, J. A., Jr.; Frisch, M. J.; Ochterski, J. W.; Petersson, G. A. *J. Chem. Phys.* **1999**, *110*, 2822.
(51) Montgomery, J. A., Jr.; Frisch, M. J.; Ochterski, J. W.; Petersson, G. A. *J. Chem. Phys.* **2000**, *112*, 6532.
(52) Woon, D. E.; Dunning, T. H. *J. Chem. Phys.* **1995**, *103*, 4572.
(53) Xu, Y. K.; Chen, Z. W.; Sun, J.; Liu, K.; Chen, W.; Shi, W.; Wang, H. M.; Zhang, X. K.; Liu, Y. *J. Org. Chem.* **2002**, *67*, 7624−7630.
(54) Villamena, F. A.; Dickman, M. H.; Crist, D. R. *Inorg. Chem.* **1998**, *37*, 1446−1453.
(55) Boeyens, J. C. A.; Kruger, G. J. *Acta Crystallogr.* **1970**, *B26*, 668.
(56) Alini, S.; Citterio, A.; Farina, A.; Fochi, M. C.; Malpezzi, L. *Acta Crystallogr.* **1998**, *C54*, 1000−1003.
(57) Mahoney, L. R.; Mendenhall, G. D.; Ingold, K. U. *J. Am. Chem. Soc.* **1973**, *95*, 8610−8614.
(58) Bartberger, M. D.; Fukuto, J. M.; Houk, K. N. *Proc. Natl. Acad. Sci. U.S.A.* **2001**, *98*, 2194−2198.
(59) Mujika, J. I.; Mercero, J. M.; Lopez, X. *J. Phys. Chem. A* **2003**, *107*, 6099−6107.
(60) Silva, C. O.; da Silva, E. C.; Nascimento, M. A. C. *J. Phys. Chem. A* **2000**, *104*, 2402−2409.
(61) Pliego, J. R.; Riveros, J. M. *J. Phys. Chem. A* **2002**, *106*, 7434−7439.
(62) To reproduce the solvent parameters of Tomasi et al. that existed in the Gaussian 94 implementation using Gaussian 98, a routine using "scrf=oldpcm" was used.
(63) Wiberg, K. B.; Laidig, K. E. *J. Am. Chem. Soc.* **1988**, *110*, 1872−1874.
(64) Wang, X.; Houk, K. N. *J. Am. Chem. Soc.* **1988**, *110*, 1870−1872.
(65) Saracino, G. A. A.; Tedeschi, A.; D'Errico, G.; Improta, R.; Franco, L.; Ruzzi, M.; Corvaia, C.; Barone, V. *J. Phys. Chem. A* **2002**, *106*, 10700−10706.
(66) Richardson, W. H.; Hodge, V. F. *J. Org. Chem.* **1970**, *35*, 4012−4016.
(67) Behar, D.; Czapski, G.; Rabani, J.; Dorfman, L. M.; Schwarz, H. A. *J. Phys. Chem.* **1970**, *74*, 3209−3213.
(68) Jonsson, M. *J. Phys. Chem.* **1996**, *100*, 6814−6818.
(69) Serjeant, E. P.; Dempsey, B. *Ionisation Constants of Organic Liquids in Aqueous Solution*; Pergamon: New York, 1979.
(70) Czapski, G.; Bielski, B. H. J. *J. Phys. Chem.* **1963**, *67*, 2180−2184.
(71) Buettner, G. R. *Arch. Biochem. Biophys.* **1993**, *300*, 535−543.
(72) Finkelstein, E.; Rosen, G. M.; Rauckman, E. J. *J. Am. Chem. Soc.* **1980**, *102*, 4995.
(73) Villamena, F.; Hadad, C. M.; Zweier, J. *J. Phys. Chem. A* **2003**, *107*, 4407−4414.